TENSILE BEHAVIOR OF A CFRP WIRE ROPE WITH INDEPENDENT CORE: ANALYTICAL AND NUMERICAL ANALYSES

Felipe F. Luz[a], Laís V. Silva[a], Sandro C. Amico[a], Carlos A. Cimini Jr.[b*]

[a]*Department of Materials Engineering, Federal University of Rio Grande do Sul*
Av. Bento Gonçalves, 9500, Bairro Agronomia, 91501-970, Porto Alegre, RS, Brazil

[b]*Department of Structural Engineering, Federal University of Minas Gerais*
Av. Antônio Carlos, 6627, Pampulha, 31.270-901, Belo Horizonte, MG, Brazil
**cimini@ufmg.br*

Keywords: composites, cables, wire rope, modeling.

Abstract
Carbon Fiber Reinforced Polymer (CFRP) wire ropes with independent wire rope core (IWRC) present outstanding performance in terms of specific stiffness and strength, and fatigue behavior. Particularly in civil engineering, CFRP single strands (1x7 configuration), spiral cables (1x19 configuration) and wire ropes (6x7 stranded configuration) have been used in many structural applications. In this study, a CFRP 6x7 wire rope with IWRC has been developed and tested for tensile behavior. Two mathematical models were studied: the first was based on the analytical theory of wire rope for isotropic materials and the second was based on a numerical approach using finite element analysis. Application of the isotropic analytical model for composite cables yielded prediction deviations close to 5% as compared to the 3D finite element numerical model, with contact hypothesis and material orthotropic orientation, for a pure tensile load.

1. Introduction

Carbon Fiber Reinforced Polymer (CFRP) cables present outstanding performance in terms of specific stiffness and strength, and fatigue [1]. Also, they can be natural candidates for harsh environments, such as offshore applications, due to their excellent corrosion-resistant properties. The introduction of CFRP instead of steel for cables has been proposed by Meier et al. [2]. From the lifetime point of view, studies indicated superior results for carbon fiber composites compared to aramid or glass, and the potential of carbon fibers is considered promising [3].

Many studies related to steel cables have been performed to evaluate their mechanical properties. Particularly for civil engineering, CFRP cables and profiles have been used for many structural applications. For instance, reinforced concrete bridge piers, which are subjected to corrosion from salty breezes, were strengthened by CFRP cables instead of reinforcing steel bars. Figure 1 shows cable strands into a cable stay bridge in Maine (USA) started in July 2003 when the Maine Department of Transportation awarded a contract for renovation of the 75-year old Waldo-Hancock (steel suspension) Bridge [4]. Studies on CFRP

cables, however, are scarce even though they are essential. Moreover, the behavior of such cables is not fully understood. Issues like the role of the orthotropic properties inherent to the material or the effect of the contact loads between the wires still need clarification.

Figure 1. CFRP Cable strands into a cable stay bridge in Maine (USA) [4].

On the contrary, the behavior of metallic wire ropes has been thoroughly studied [5-7]. Analytical models take into account the geometry of the component as well as the hypothesis of contact between the wires. Yet, these models were developed for isotropic materials and there are no such models available for composites.

In this study, a commercial CFRP cable previously tested for tensile behavior was selected to verify the accuracy of two mathematical models. The first model was based on the analytical theory of wire rope for isotropic materials presented by Costello [6], and the second one was based on finite element analysis.

2. Analytical Model

The analytical model used in this study is thoroughly explained in Costello [6]. The 1×7 cable is the sub-element of more complex wire ropes, such as the 6×7 cable. This model is then based in the use of kinematics of a thin wire to get the equilibrium equations (Equations 1-6):

$$\frac{dN}{dS} - N'\tau + T\kappa' + X = 0 \tag{1}$$

$$\frac{dN'}{dS} - T\kappa + N\tau + Y = 0 \tag{2}$$

$$\frac{dT}{dS} - N\kappa' + N'\kappa + Z = 0 \tag{3}$$

$$\frac{dG}{dS} - G'\tau + H\kappa' - N' + K = 0 \tag{4}$$

$$\frac{dG'}{dS} - H\kappa + G\tau - N + K' = 0 \tag{5}$$

$$\frac{dH}{dS} - G\kappa' + G'\kappa + \Theta = 0 \tag{6}$$

where N and N' are the components of the shearing force on a wire cross section in the *x* and *y* directions, respectively; τ is the twist per unit length; T is the axial tension in the wire; X, Y, Z are the components of the external line load per unit length of the centerline of the wire in the *x*, *y* and *z* directions, respectively; κ and κ' are the components of curvature in the *x* and *y* directions, respectively; G and G' are the components of the bending moment on a wire cross-section in the *x* and *y* directions, respectively; H is the twisting moment in the wire; K, K' and Θ are the components of the external moment per unit length of the centerline in the *x*, *y* and *z* directions, respectively. Figure 2 shows the loads acting on an helical wire of a 1×7 strand.

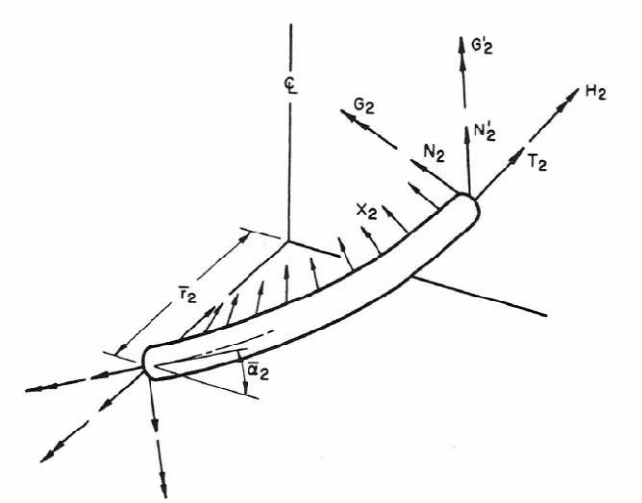

Figure 2. Loads acting on a helical wire [6].

The final equations for a static response for a 1×7 strand [6] are described by Equations 16-26, where E is the elastic modulus and ν is the Poisson's ratio of the wire for an isotropic material.

$$\frac{G'_2}{ER_2^3} = \frac{\pi}{4} R_2 \Delta\kappa'_2 \tag{7}$$

$$\frac{H_2}{ER_2^3} = \frac{\pi}{4(1+\nu)} R_2 \Delta\tau_2 \tag{8}$$

$$\frac{N'_2}{ER_2^2} = \frac{H_2}{ER_2^3} \frac{\cos^2\alpha_2}{r_2/R_2} - \frac{G'_2}{ER_2^3} \frac{\operatorname{sen}\alpha_2 \cos\alpha_2}{r_2/R_2} \tag{9}$$

$$\frac{T_2}{ER_2^2} = \pi\xi_2 \tag{10}$$

$$\frac{X_2}{ER_2} = \frac{N'_2}{ER_2^2} \frac{\operatorname{sen}\alpha_2 \cos\alpha_2}{r_2/R_2} - \frac{T_2}{ER_2^3} \frac{\cos^2\alpha_2}{r_2/R_2} \tag{11}$$

$$\frac{F_2}{ER_2^2} = m_2 \left[\frac{T_2}{ER_2^2} \operatorname{sen}\alpha_2 + \frac{N'_2}{ER_2^2} \cos\alpha_2 \right] \tag{12}$$

$$\frac{M_2}{ER_2^3} = m_2 \left[\frac{H_2}{ER_2^3} \operatorname{sen}\alpha_2 + \frac{G'_2}{ER_2^3} \cos\alpha_2 + \frac{T_2}{ER_2^2} \frac{r_2}{R_2} \cos\alpha_2 - \frac{N'_2}{ER_2^2} \frac{r_2}{R_2} \operatorname{sen}\alpha_2 \right] \tag{13}$$

$$\frac{F_1}{ER_1^2} = \pi\xi_1 \tag{14}$$

$$\frac{M_2}{ER_1^3} = \frac{\pi}{4(1+\nu)} R_1\tau_s \tag{15}$$

$$F = F_1 + F_2 \tag{16}$$

$$M_t = M_1 + M_2 \tag{17}$$

Figure 3 shows the cross section of a 6×7 cable. For the solid wire strands in strand 1, the twisting moment and the axial force in the strands are determined from the properties of a straight solid wire with an angle of twist per unit length of $\Delta\tau_2$, that is, $H = \pi ER_2^4\Delta\tau_2/4(1+\nu)$ and $T = \pi ER_2^2\xi_2$. Thus, the axial strain and the angle of twist per unit length will be used to determine the axial force and axial twisting moment in the curved strand. Let the helix angle of strand 2, shown in Figure 3, be α_2^*. As the rope is loaded, this helix angle assumes a new value $\bar{\alpha}_2^*$. The angle of twist per unit length for strand 2 becomes

$$\Delta\tau_2^* = \frac{\operatorname{sen}\bar{\alpha}_2^*\cos\bar{\alpha}_2^*}{\bar{r}_2^*} - \frac{\operatorname{sen}\alpha_2^*\cos\alpha_2^*}{r_2^*} \tag{18}$$

in which:

$$r_2^* = R_1 + 2R_2 + 2R_4 + R_3 \tag{19}$$

and where, due to Poisson's ratio effect,

$$\bar{r}_2^* = r_2^* - \nu(R_1\xi_1 + 2R_2\xi_2 + 2R_4\xi_4 + R_3\xi_3) \tag{20}$$

in which ξ_1, ξ_2, ξ_3 and ξ_4 are the axial wire strains in wires 1, 2, 3, 4, respectively.

Guided by the analyses of strand 1 the following equations can be written:

$$\xi_1 = \xi_3 + \frac{\Delta A_4^*}{\tan A_2^*} \tag{21}$$

$$\xi_3 = \xi_4 + \frac{\Delta A_4}{\tan A_4} \tag{22}$$

$$R_2^*\tau = \frac{\xi_3}{\tan A_2^*} - \Delta A_2^* + \frac{\nu}{R_2^*}\frac{(R_1\xi_1 + 2R_2\xi_2 + 2R_4\xi_4 + R_3\xi_3)}{\tan A_2^*} \tag{23}$$

$$\begin{aligned}(R_3 + R_4)\Delta\tau_2^* = \frac{(R_3+R_4)}{R_2^*}\Bigg[&(1-2\operatorname{sen}^2 A_2^*)\Delta A_2^* \\ &+ \nu\frac{(R_1\xi_1 + 2R_2\xi_2 + 2R_4\xi_4 + R_3\xi_3)}{R_2^*}\operatorname{sen}A_2^*\cos A_2^*\Bigg]\end{aligned} \tag{24}$$

where τ is the twist per unit length of the rope and $\Delta\tau_2^*$ is the angle of twist per unit length of strand 2.

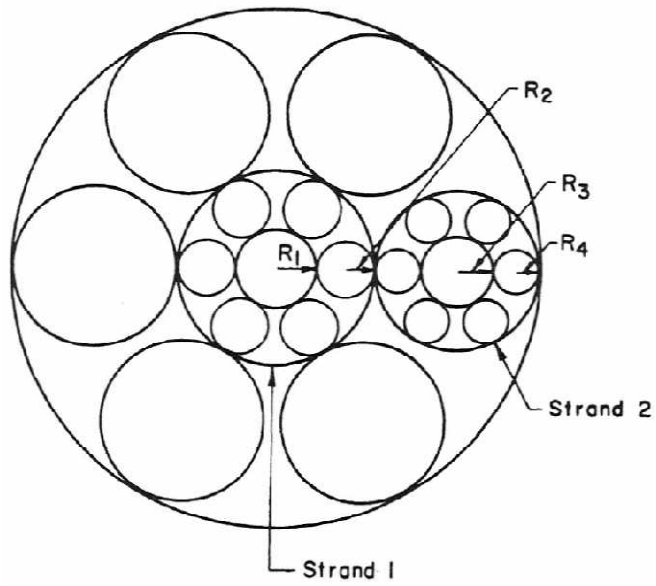

Figure 3. Cross section of a 6×7 cable [6].

The final equations for the analytical model for the 6×7 cable are given by Equations (25-30).

$$G'^*_2 = A^*_2 \Delta\kappa^*_2 = A^*_2 \left(\frac{\cos^2 \overline{\alpha}^*_2}{r^*_2} - \frac{\cos^2 \alpha^*_2}{r^*_2} \right) \tag{25}$$

$$N'^*_2 = H^*_2 \frac{\cos^2 \alpha^*_2}{r^*_2} - G'^*_2 \frac{\operatorname{sen} \alpha^*_2 \cos \alpha^*_2}{r^*_2} \tag{26}$$

$$F^*_2 = 6(T^*_2 \operatorname{sen} \alpha^*_2 + N'^*_2 \cos \alpha^*_2) \tag{27}$$

$$M^*_{12} = 6(H^*_2 \operatorname{sen} \alpha^*_2 + G'^*_2 \cos \alpha^*_2 + T^*_2 r^*_2 \cos \alpha^*_2 - N'^*_2 r^*_2 \operatorname{sen} \alpha^*_2) \tag{28}$$

$$F = F^*_1 + F^*_2 \tag{29}$$

$$M_t = M^*_{t1} + M^*_{t2} \tag{30}$$

In the current study, the 6×7 strand is in fact a composite material. Since the cable performance under tensile loading will be dominated by the axial properties, a simplified approach was adopted by merely using the equivalent axial composite modulus (E_1) and Poisson's ratio (ν_{12}) instead of the corresponding isotropic properties (E and ν, respectively).

3. Numerical Model

The numerical model was developed within the commercial finite element platform Abaqus™. The 6×7 strand was created with wire diameter of 3 mm, cable nominal diameter of 27 mm, 100 mm length and pitch of 1000 mm and double pitch of 3000 mm with the

regular lay orientation (Figure 4). The material properties used were those shown in Table 1. Each wire in the strand has its material orientation fiber axis set along the helix length, as seen in Figure 4b, and in a single spring in Figure 4a. The mesh is comprised of 8-node tetrahedral elements type C3D10, with a total of 15,777 nodes and 53,087 elements (Figure 5).

E_1 = 147.6 GPa	G_{12} = 2.87 GPa	ν_{12} = 0.28
E_2 = 8.6 GPa	G_{13} = 2.87 GPa	ν_{13} = 0.28
E_3 = 8.61 GPa	G_{23} = 3.60 GPa	ν_{23} = 0.02

Table 1. Elastic constants for CFRP used in the models.

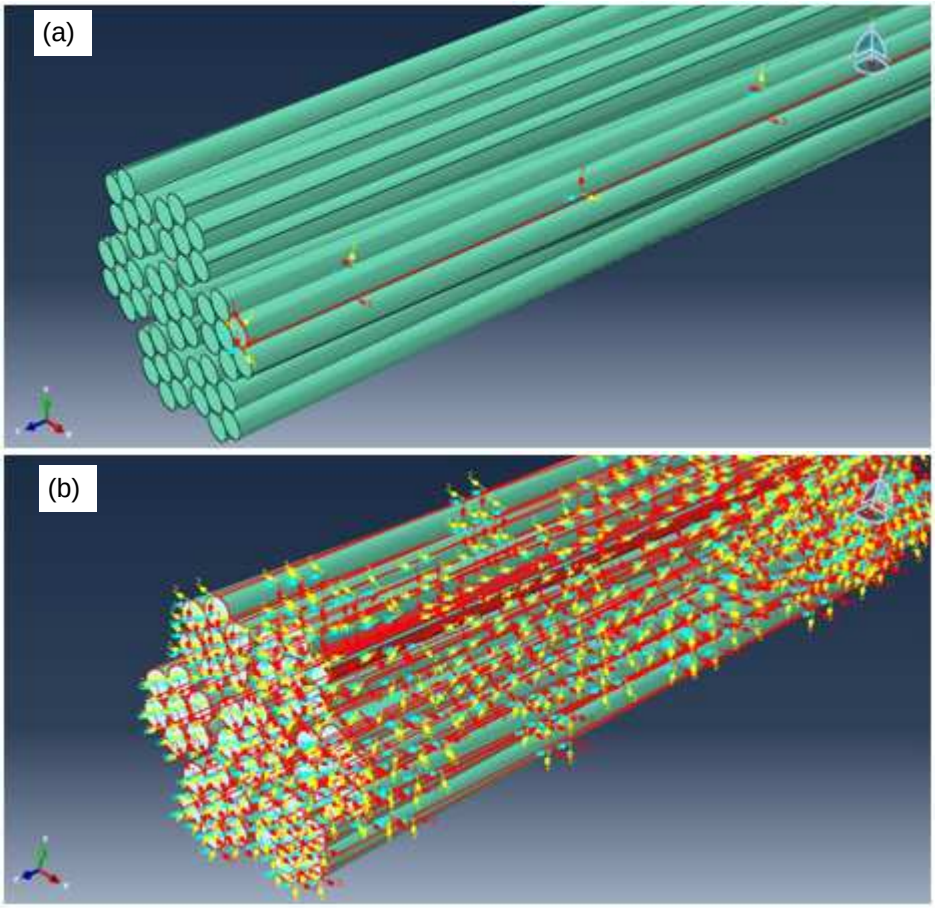

Figure 4. Description of material orientation (fiber axis) along the helix length: (a) for a single wire and (b) for the 6×7 cable.

Contact hypothesis was assumed between the wires, node-to-surface discretization method was applied with small sliding allowed on a total of 96 contact pairs. The contact properties have been set with a tangential behavior, with a friction coefficient of 0.6, and with normal behavior with pressure-overclosure set as “hard” contact. One of the strand ends was built-in, not allowing deflection or rotation in any direction. On the other end, rotation around the z axis was allowed in the longitudinal direction of the strand (fixed-end, $\tau = 0$), and the axial force was applied at this same end.

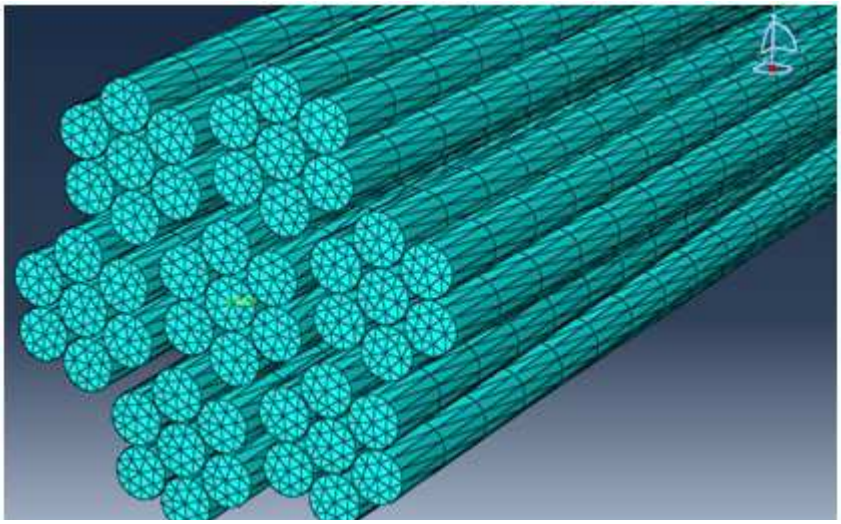

Figure 5. 3D numerical model of the CFRP cable: Mesh with 8-node tetrahedral elements.

4. Results

Tensile predictions of analytical and numerical models results for the CFRP 6×7 cable is presented in Figure 6. Table 2 shows the tensile stiffness and failure load for comparison. It can be seen that the analytical model overestimated the numerical model stiffness by 4.50% and failure load by 4.46%. This indicates that this model, in spite of be originally developed for isotropic cables, showed small errors compared to the numerical model developed for orthotropic cables for a pure tensile load. The mere replacement of the elastic properties did generate a reliable result, presenting errors inferior to 5%. Furthermore, these results did not need for hard computational processing, due to the low complexity of the equations involved and the simplified hypothesis of no contact used. Simulations for the 3D numerical model were performed in a 4-core i5 processor with 6 MB RAM memory, taking about 180 min to run. This model has a higher complexity compared to the analytical model, since it includes 3D geometry, contact hypothesis and correct orthotropic material characterization and orientation, but demands greater computational effort.

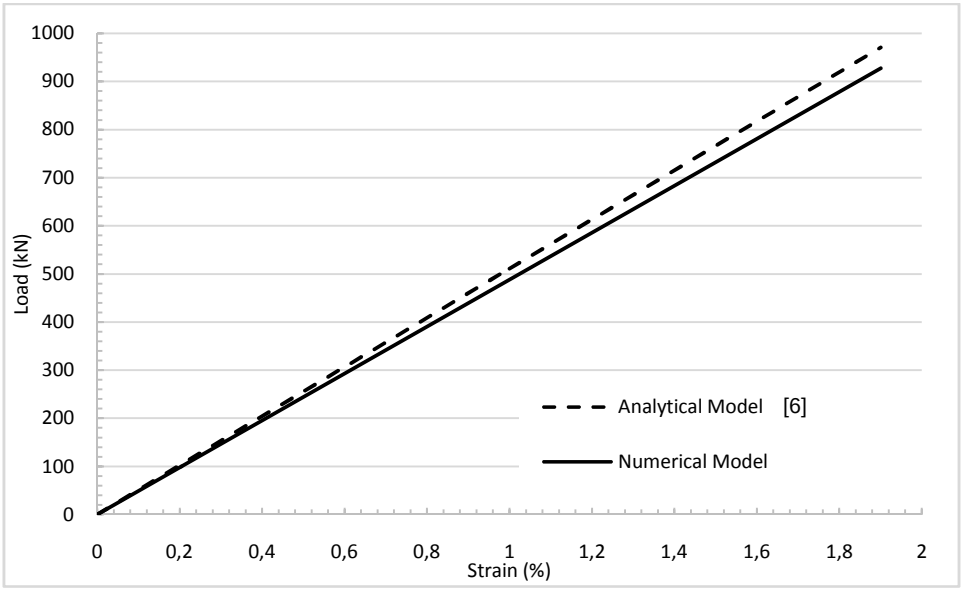

Figure 6. Load *vs.* Strain curves for the CFRP 6×7 cable for the numerical model and analytical model.

Model	Stiffness (kN/m^2)	Difference (%)	Failure load (kN)	Difference (%)
Analytical Model	510	4.50	970.28	4.46
Numerical Model	488	-	927.00	-

Table 2. Tensile stiffness and failure load for the 6×7 CFRP cable.

5. Conclusions

CFRP cables have a great potential to be applied in different engineering fields for high performance applications. No analytical model dedicated for composite cables could be found in the literature. Use of the isotropic model considering the equivalent axial composite modulus (E_1) Poisson's ratio (ν_{12}) instead of the corresponding isotropic properties (E and ν, respectively), generated differences smaller than 5% in comparison with the numerical model. However, the 3D numerical model is more complex considering contact hypothesis and material orthotropic orientation.

Acknowledgements

Authors would like to acknowledge the support of UFRGS, CNPq, CAPES and FAPEMIG.

References

[1] U. Meier. Carbon Fiber Reinforced Polymer Cables: Why? Why Not? What If? *Arabian Journal for Science and Engineering*, 37:399-411, 2012.

[2] U. Meier, R. Müller and A. Puck. GFK-Biegeträger Unter Quasistatischer und Schwingender Beanspruchung. In: *Proceedings of Internationale Tagung Über Verstärkte Kunststoffe*, 35.1-35.7, 1982.

[3] U. Meier. Carbon Fiber Reinforced Polymers: Modern Materials in Bridge Engineering. *Structural Engineering International*, 2:71-2, 1992.

[4] W. J. Rohleder Jr., B. Tang, T. A. Doe, N. F. Grace and C. J. Burgess. CFRP Strand Application on Penobscot Narrows Cable Stayed Bridge. *Transportation Research Board Journal*, 1-15, 2008.

[5] G. A. Costello and S. K. Sinha. Static behavior of wire rope. ASCE *Journal of the Engineering Mechanics Division*, 103:1011-1022, 1977.

[6] G. A. Costello. *Theory of Wire Rope*. Mechanical Engineering Series, 2nd Edition, Springer-Verlag, New York, 1997.

[7] K. Kumar, J. E. Cochran Jr. and J. A. Cutchins. Contact Stresses in Cables Due to Tension and Torsion. *Journal of Applied Mechanics*, 64:935-939, 1997.